The phase behaviour of cetyltrimethylammonium chloride aqueous solutions at high concentrations: An all-atom Molecular Dynamics simulation study

Flora D. Tsourtou, Stavros D. Peroukidis and Loukas Peristeras*

Institute of Nanoscience and Nanotechnology, Molecular Thermodynamics and Modelling of Materials Laboratory, National Center for Scientific Research "Demokritos", GR-15310 Agia Paraskevi Attikis, Greece. E-mail: l.peristeras@inn.demokritos.gr

Electronic Supplementary Information (ESI)

The supplementary information file is organised as follows: In section S.1, the procedure followed in the molecular dynamics (MD) simulations of the hexagonal columnar phase (H_1), is described. Details for the selection of the force-field, are provided in Section S.2. The dependence of the characteristic distances of the radial density profiles on the micellar size is further demonstrated in the figures presented in Section S.3. Finally, in Section S.4, the time evolution of micelles and the observation of merge/split events in the micellar phase (L_1), are presented.

S.1 Simulations of the hexagonal columnar phase (H_1)

In molecular simulations, a perfect hexagonal columnar phase may occur only in simulation cells consistent with the space group of the underlying structure. Therefore, they should be multiples of unit cells with vertices that project on the points of the 2d hexagonal lattice. Consequently, cylindrical columns occurring during the simulation are either parallel to the space or face diagonals of the cell or normal to its faces. In the former case, the vertices of the diagonal(s) parallel to the columns project at the same lattice point, while in the latter case one face of the cell coincides with a unit cell of the 2D hexagonal lattice. In this work, we refer to the orthogonal simulation cells able to host the H_1 phase as type I, II and III depending whether the formed columns are parallel to the space diagonals, parallel to the face diagonals or normal to the faces of the cell, respectively (see Fig. **S1**).

Fig. S1: The types of orthogonal simulation cells able to host the H_1 phase. The cylindrical columns are normal to the page and are illustrated with the grey circles; their centres define the points of the 2d hexagonal lattice. The apexes of each unit cell are projected on these lattice points. Type-I cells (coloured red) are cubic and host cylinders parallel to their space diagonal. Type -II cells (coloured orange) host columns parallel to their face diagonals. Type-III cells (coloured purple) host columns normal to their faces. The primitive cell (coloured black) of the 2d hexagonal lattice is also illustrated.

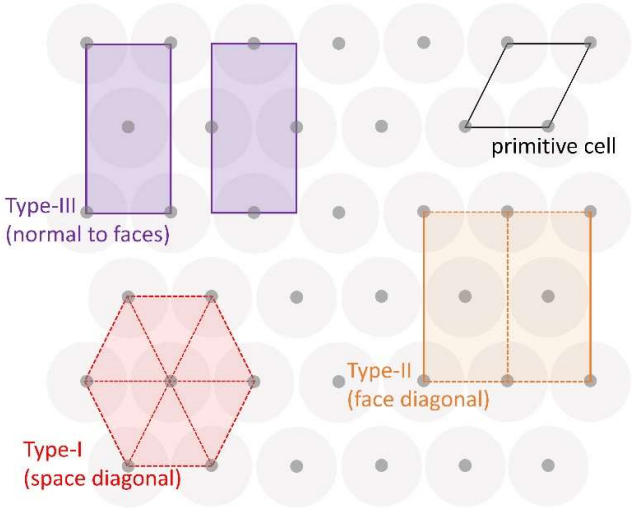

The size of the unit cells of the H_1 phase are defined from the spacing of the lattice d (i.e., the height of the primitive cell):

primitive cell	$\alpha = a = b = c$ $\alpha = \beta = 90°,\ \gamma = 120°$	$\alpha = \frac{2}{\sqrt{3}} d$	(1)
unit cell type I	$a = b = c$ $\alpha = \beta = \gamma = 90°$	$a = \sqrt{\frac{3}{2}}\, d$	(2)
unit cell type II	$a\ ,\ b\ ,\ c$ $\alpha = \beta = \gamma = 90°$	$a \in \mathbb{R}^+ : a > \frac{2}{\sqrt{3}} d\ ,\ b = \frac{2\,a\,d}{\sqrt{3\,a^2 - 4\,d^2}}\ ,$ $c = n 2d, n \in \mathbb{N}^+$	(3)
unit cell type III	$a\ ,\ b\ ,\ c$ $\alpha = \beta = \gamma = 90°$	$a = \alpha\ ,\ b = 2d\ ,\ c \in \mathbb{R}^+$	(4)

Please note that normal Greek letter alpha (α) denotes the distance between column centers i.e., the edge length of the primitive cell and italic Greek letter alpha (α) denotes the angle between a and b edges.

The dependency of the spacing d of the hexagonal lattice from concentration of CTAC is given by the formula:

$$d = \sqrt{\frac{\rho_L M}{\rho w} \frac{\sqrt{3}}{2} ct} \tag{5}$$

where, ρ_L is the molecular density along the axis of the column (linear density, in molecules Å^{-1}), w is the percent by mass concentration of CTAC (wt%), ρ is the mass density of the system (in g cm^{-3}), M is the molecular weight of CTAC (in g mol^{-1}), and ct a convention factor for the units ($ct = N_A^{-1} 10^{26}$ Å^3 cm^{-3}). Given the concentration, the mass density of the system and the linear density of cylindrical columns, d is obtained directly from eq. 5 and in turn, all the details of the simulation cell (i.e., size and number of molecules of the molecular species) can be specified. Moreover, if the dependence of d and ρ on w is known (e.g., from XRD experiments), then ρ_L can be calculated using eq. 5 and expressed also as a function of the concentration.

In this study, it is assumed that the density of the system changes marginally with concentration and that the value of the linear density of the cylindrical columns in the H_1 phase is similar to the corresponding values observed for the rod-like micelles in the micellar phase (L_1). From the simulation at the lower concentration considered (34.1 wt%), it was estimated that ρ=0.971 g cm^{-3} and ρ_L=2.18±0.12 Å^{-1}. For the rest of the concentrations, a reasonably lower value for the mass density is assumed (0.95 g cm^{-3}) and the linear density was scaned in the range from 1.9 up to 2.4 Å^{-1} with step 0.1 Å^{-1}, to test if the H_1 phase can be obtained. However, the nominal values of the linear density used for the construction of the initial configurations, were adjusted per case and in order to achieve a difference of 10, 15 or 20 CTAC molecules between two adjacent ρ_L values. For each concentration, five (5) trial initial configurations were tested per linear density value. If none of the trials resulted in the H_1 phase, it is considered that H_1 phase does not occur in the corresponding linear density. In turn, if the H_1 phase exhibited in none of the linear densities, it is then concluded that the micellar phase does not occur for the specific concentration. Consequently, for even lower concentrations only the micellar phase is expected. The details of the type I simulation cells were determined using eq. 5 and eq. 2 as described above and are reported in **Table S1**.

Table S1: Details of the systems examined for each concentration considered. For w =50.0% the linear density of 2.4 Å $^{-1}$ was not tested since at w =57.6% the H_1 phase does not occur for this value. For concentrations lower than 50.0%, the tests were omitted since none of the linear density values resulted in the H_1 phase occurrence for this specific concentration. Based on the tests' results, one extra nominal value of linear density was examined for the concentrations of 65.5 and 70.5 wt% to achieve lower shear stress values.

	50.0 wt%		57.6 wt%		65.5 wt%		70.5 wt%	
ρ_L (Å^{-1})	# CTAC	# WATER	# CTAC	# WATER	# CTAC	# WATER	# CTAC	# WATER
1.9	190	3035	190	2485	190	1780	165	1225
2.0	210	3355	200	2620	200	1870	180	1340
2.1	225	3600	215	2810	210	1960	195	1450
2.18	-	-	-	-	215	2010	-	-
2.2	240	3845	230	3000	220	2055	210	1565
2.3	255	4085	245	3200	230	2155	225	1670
2.36	-	-	-	-	-	-	233	1731
2.4	-	-	260	3400	240	2245	240	1780

For the concentrations of 57.6, 65.5, and 70.5 wt%, the H_1 phase occurred for the tested values of the linear density. At 57.6 wt%, only for ρ_L =2.4 Å^{-1} the H_1 phase was not formed, while for ρ_L =2.3 Å^{-1} and in spite of the obtained hexagonal lattice, the columns resembled the threaded shank of a screw object. However, for w =50.0 wt%, none of the tests resulted in the hexagonal columnar phase. For each concentration and linear density values, one of the trial systems, where the H_1 phase was demonstrated, was further equilibrated applying step 4 of the calculation workflow (see main manuscript). The mean values of the linear density calculated from the MD simulation are reported in **Table S2** for each concentration and they are close to their nominal values. The obtained structural and thermodynamic properties of the equilibrated test systems were very similar independent of the corresponding value of the linear density. For example, the potential energy per molecule and the density of the systems (see **Table S2**) were roughly the same although a marginal reduction in their values (less than 0.05%) was observed as the linear density increases; moreover, the pressure was equilibrated to the pre-set value of 1 atm.

Table S2: The mean of the linear density , the mean potential energy per molecule ($\langle U \rangle$) and the mean mass density of the system, as calculated from the MD simulations of the systems corresponding to the various test values of the nominal linear density (ρ_L) examined for each concentration considered in the H_1 phase region. The test systems where no shear stresses were present are highlighted in grey.

57.6 wt%			65.5 wt%			70.5 wt%		
$\langle \rho_L \rangle$ (Å^{-1})	$\langle U \rangle$ (kJ/mol)	$\langle \rho \rangle$ (g/cm^3)	$\langle \rho_L \rangle$ (Å^{-1})	$\langle U \rangle$ (kJ/mol)	$\langle \rho \rangle$ (g/cm^3)	$\langle \rho_L \rangle$ (Å^{-1})	$\langle U \rangle$ (kJ/mol)	$\langle \rho \rangle$ (g/cm^3)
1.91±0.03	-59.633±0.002	0.9522±10^{-4}	1.90±0.03	-65.881±0.003	0.9461±10^{-4}	1.85±0.03	-71.028±0.003	0.9422±10^{-4}
1.97±0.03	-59.621±0.003	0.9525±10^{-4}	1.99±0.04	-65.949±0.002	0.9462±10^{-4}	1.95±0.04	-71.016±0.005	0.9424±10^{-4}
2.05±0.05	-59.678±0.001	0.9528±10^{-4}	2.04±0.04	-65.978±0.005	0.9464±10^{-4}	2.06±0.03	-71.103±0.004	0.9427±10^{-4}
2.15±0.04	-59.727±0.002	0.9529±10^{-4}	2.15±0.04	-65.999±0.002	0.9465±10^{-4}	2.16±0.04	-71.082±0.009	0.9429±10^{-4}
2.26±0.04	-59.633±0.002	0.9532±10^{-4}	2.20±0.04	-66.037±0.009	0.9466±10^{-4}	2.26±0.04	-71.219±0.004	0.9431±10^{-4}
-	-	-	2.24±0.03	-65.983±0.005	0.9467±10^{-4}	2.33±0.04	-71.172±0.004	0.9426±10^{-4}
-	-	-	2.40±0.04	-66.038±0.005	0.9472±10^{-4}	2.38±0.04	-71.267±0.003	0.9433±10^{-4}

Nevertheless, this was not the case for the off-diagonal elements of the pressure tensor since their values change drastically with linear density (see **Fig. S2**b). If the mean of their absolute values, $\left(\left|p_{xy}\right|+\left|p_{xz}\right|+\left|p_{yz}\right|\right)/3$, is considered a smooth function of linear density, its minimum should be equal to zero, a value that indicates the absence of shear stresses (see **Fig. S2**a). In this study and for each concentration examined, this minimum is located within the range of linear density values tested, and it was approximated by the specific ρ_L test value where the function obtained its minimum value. This specific value conforms to the equilibrium ensemble of the conducted MD simulations and corresponds to the thermodynamic state point, which otherwise is fully defined by the composition of the aqueous solution (given the temperature and the pressure). For the obtained hexagonal columnar phase, the results presented in the main manuscript for each concentration were extracted from the simulation in which no shear stresses are present. For the concentrations of 65.5 and 70.5 wt%, one extra simulation was conducted to achieve lower values for the shear stresses at nominal linear density values of 2.18 and 2.36 $Å^{-1}$, respectively.

Fig. S2: (a) The mean of the absolute values, and (b) the actual values of the off-diagonal elements of the pressure tensor calculated from the *NPT* MD simulations as function of the value of the linear density tested for the three concentrations where the H_1 phase occurs. The minimum of $\left(\left|p_{xy}\right|+\left|p_{xz}\right|+\left|p_{yz}\right|\right)/3$ as a function of the linear density is expected to be found in the regions highlighted with grey colour in the diagrams (b).

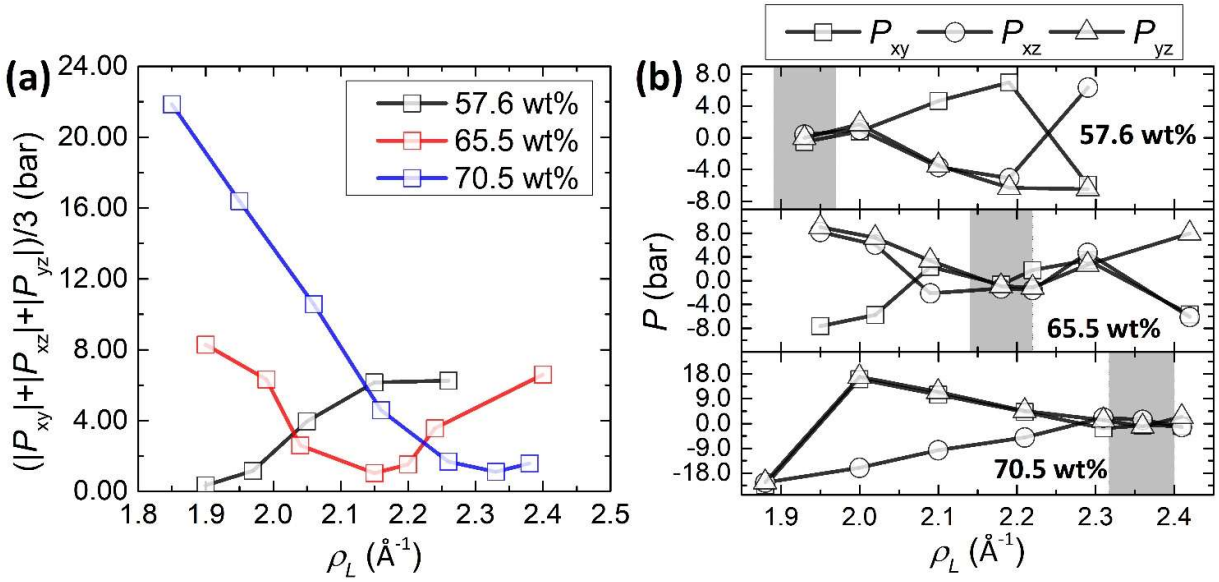

The structure of the cylindrical columns in all cases, was analysed by means of radial density profiles (see Section **3.1** in the main manuscript). The positions of the profiles and consequently the values of the corresponding characteristic distances depend on both the concentration and the linear density. For each concentration, the values of $R_{W\text{-}H}$, R_H, and R_{Cl} increase linearly with linear density (see **Fig. S3**). Moreover, for a given linear density and independent of the specific value, the peak of the head distributions change marginally with concentration; its value reduces around 0.5 Å when going from 57.6 to 70.5 wt% (see **Fig. S3**); for the same range of concentrations, the value of R_{Cl} distance reduces drastically by around 2.0 Å. On the contrary, $R_{W\text{-}H}$, in practise, is not affected from the concentration for a given value of the linear density.

Fig. S3: The characteristic distances of the density profiles calculated from the linear density test simulation for each of the concentrations where the hexagonal columnar phase was obtained. $R_{W\text{-}H}$, R_H, and R_{Cl} distances are coloured black, red, and blue, respectively. Open squares, circles, and triangles are used for the concentrations 57.6, 65.5, and 70.5 wt%, respectively. The vertical dashed lines indicate the linear density value where no shear stresses are exhibited in the system for the specific concentrations used as labels. For clarity, symbols of larger size with crosses at their centres are utilized to mark the points where shear stresses are absent.

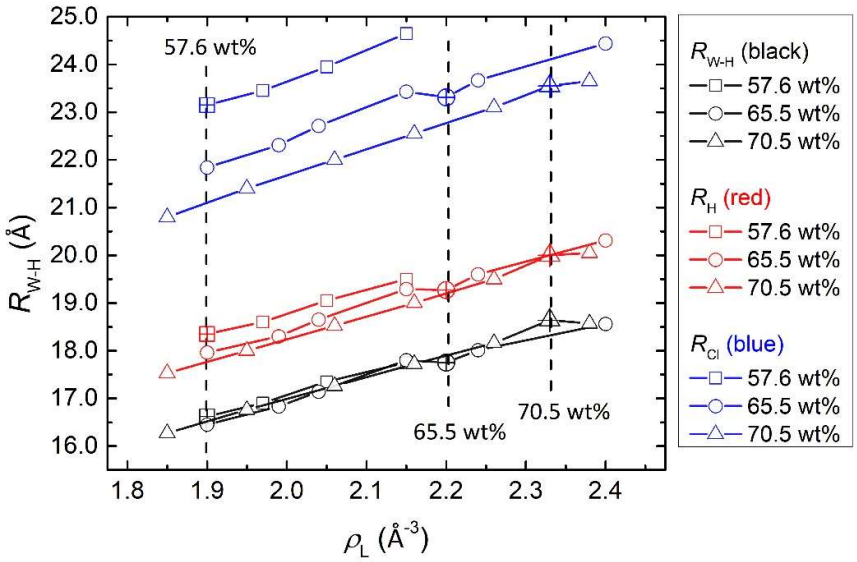

S.2 Force field selection

The electrostatic interactions between the head of the surfactant molecules, the counter anions, and the water molecules define the properties of the micellar phase as well as the mesophases that occur in surfactant aqueous solutions. [1-3] The CGenFF[4], the GAFF-AA[5], and the AA-OPLS[6] are three of the most widely used AA force fields for modelling systems of biological interest. For CTAC, they assign a total head charge value equal to 0.61, 0.58, and 0.75 e^-, respectively (set **Table S3**). If C_{16} methyl group (see Fig. 1a of the main manuscript) is included as part of the head these values become 1.0 e^- for CGenFF and 0.89 e^- for the others. Given that preliminary MD simulations indicated that all the three force fields are able to predict the H_1 phase at a concentration of 65.5 wt% and 45 °C, the CGENFF was selected since the positive charge is fully located at the head moiety. It should be noted that one of our goals was the development of an algorithm suitable for the identification and the analysis of the self-assemblies formed in the simulation cell, independent of the specific force field in use.

Table S3: The charges of the head and alkyl tails for the various force fields examined (see Fig. 1a of the main manuscript). In the parenthesis, the corresponding values of C_{16} are reported, with the bonded hydrogens considered as part of the head.

OPLS-AA	GAFF (BCC charges)	CGENFF
Head's heavy (C, N) atoms charge		
-0.5 (-0.63)	-0.34 (-0.22)	-1.64 (-1.75)
Head's H atoms charge		
1.24 (1.52)	0.91 (1.11)	2.25 (2.75)
Head's total charge		
0.75 (0.89)	0.58 (0.89)	0.61 (1.0)
Tail's total charge		
0.25 (0.11)	0.42 (0.11)	0.39 (0.0)

S.3 Characteristic distances of radial density profiles as a function of the micellar size

The diagrams presented in this section of SI were constructed by tracing the characteristic distances $R_{T\text{-}W}$, R_H and R_{Cl} on the radial profiles calculated as function of their aggregation number (N_{agg}). A bin of 10 molecules was used for N_{agg}. For spherical micelles (**Fig. S4)**, the radius depends linearly on N_{agg} in the range $60 \leq N_{agg} \leq 160$. On the other hand, the radius of rod-like micelles reaches a plateau value of 20.1±0.7 for $120 \leq N_{agg} \leq 220$ (**Fig. S5)**. Micelles with N_{agg} >225 as subjected to large shape fluctuation of their couture along their elongated axis (as also verified by visual inspection). This leads to higher R_H values for N_{agg} >220 reported in **Fig. S5**b that are were excluded for the estimation of the plateau value.

Fig. S4: The dependence of (a) $R_{T\text{-}W}$, (b) R_H, and (c) R_{Cl} on the size of a spherical micelles as obtained from the radial number density profiles of molecular moieties, calculated from the MD simulations at P = 1 atm and T = 318 K for all the studied concentrations. The dashed lines are plots for the linear fits using the data from all concentrations for micellar sizes range from 60 to 130 CTAC molecules.

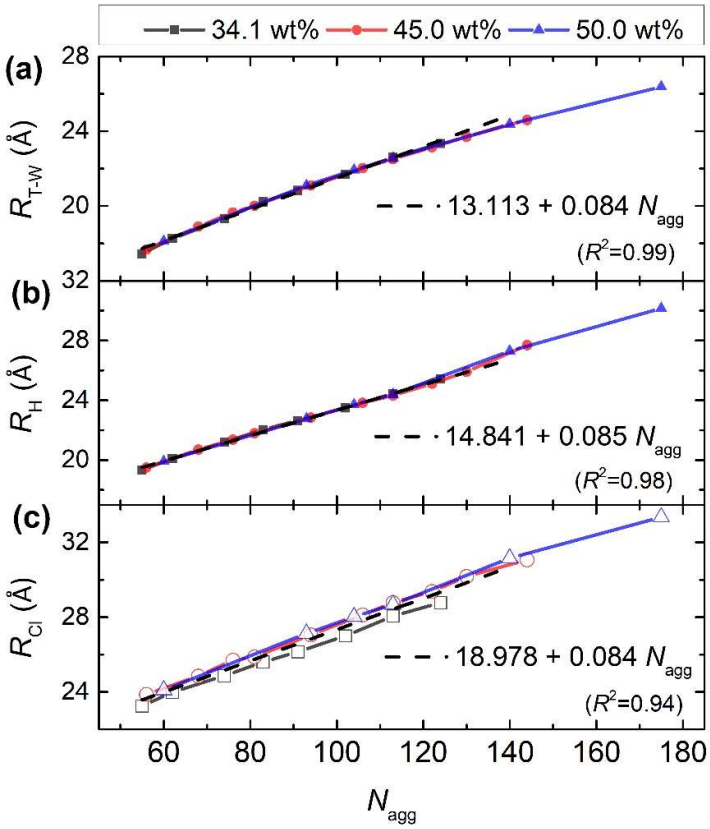

Fig. S5: The dependence of (a) $R_{T\text{-}W}$, (b) R_H, and (c) R_{Cl} on the size of a cylindrical micelles as obtained from the radial number density profiles of molecular moieties, calculated from the MD simulations at P = 1 atm and T = 318 K for all the studied concentrations. The horizontal black lines have been placed to guide the eye with respect to the mean value of the characteristic distance in the region they extend to.

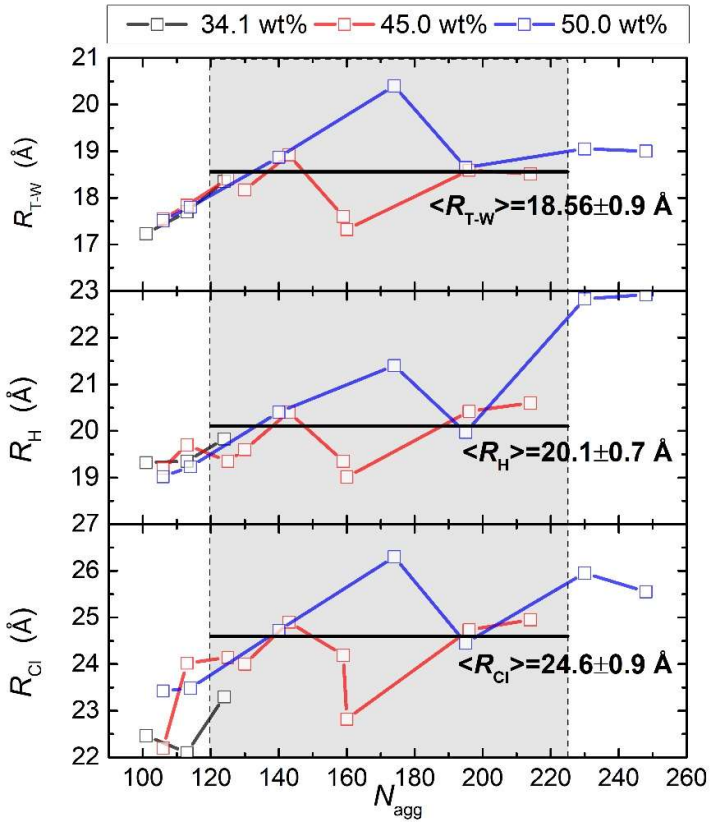

S.4 Time evolution of the micelles in the L_1 phase

In the production *NPT* simulations of the systems found in the micellar phase, a small number of events was observed and reported in **Table S4**, where two small micelles merged in a larger one (merge event) or the reverse where a large micelle spitted into two smaller ones (split event). The majority of these events were followed by their reverse in less than 100 ps. Nevertheless, rare events where the resulted micelles remain stable until the end of the simulation were also traced (marked with bold in **Table S4**) and one event where a CTAC molecule is exchanged between two micelles (marked with italic in **Table S4**). In **Table S5** these events and the occurrence time are reported, denoting a micelle as CTAC_N_{agg} where N_{agg} is the aggregate number of the micelle (e.g., CTAC_100 denotes a micelles consists of 100 CTAC molecules).

Table S4: The split and merge events traced in the simulations of the L_1 phase during the production runs. The events during which a permanent split or merge takes place are marked with bold style, while the event where a CTAC molecule exchange between micelles occurs is marked with italic style.

Time (ns)	Event
	34.1 wt%
27.24	CTAC_125 + CTAC_13 → CTAC_138
27.32	CTAC_138 → CTAC_125 + CTAC_13
65.08	CTAC_38 + CTAC_13 → CTAC_51
65.12	CTAC_51 → CTAC_38 + CTAC_13
103.88	**CTAC_38 + CTAC_13 → CTAC_51**
	45.0 wt%
20.2	CTAC_194 → CTAC_98 + CTAC_96
20.28	CTAC_98 + CTAC_96 → CTAC_194
21.72	***CTAC_194 + CTAC_109 → CTAC_193 + CTAC_110***
23.52	CTAC_193 → CTAC_97 + CTAC_96
23.60	CTAC_97 + CTAC_96 → CTAC_193
23.72	**CTAC_193 → CTAC_97 + CTAC_96**
113.76	**CTAC_215 → CTAC_108 + CTAC_107**
	50.0 wt%
15.72	CTAC_230 → CTAC_116 + CTAC_114
15.76	CTAC_116 + CTAC_114 → CTAC_230
17.28	CTAC_230 → CTAC_116 + CTAC_114
17.32	CTAC_116 + CTAC_114 → CTAC_230
17.88	**CTAC_230 → CTAC_116 + CTAC_114**
28.12	CTAC_249 → CTAC_126 + CTAC_123
28.16	CTAC_126 + CTAC_123 → CTAC_249
30.00	CTAC_390 + CTAC_114 → CTAC_504
30.08	**CTAC_504 → CTAC_390 + CTAC_114**
106.12	CTAC_106 + CTAC_61 → CTAC_167
106.16	CTAC_167 → CTAC_106 + CTAC_61
115.36	CTAC_390 → CTAC_197 + CTAC_193
115.40	CTAC_197 + CTAC_193 → CTAC_390
116.28	CTAC_390 → CTAC_197 + CTAC_193
116.32	CTAC_197 + CTAC_193 → CTAC_390

Notes and References

1. J. N. Israelachvili, D. J. Mitchell and B. W. Ninham, *Journal of the Chemical Society, Faraday Transactions 2*, 1976, **72**, 1525.
2. R. Nagarajan and E. Ruckenstein, *Langmuir*, 1991, **7**, 2934-2969.
3. E. Blackmore and G. Tiddy, *Liquid Crystals*, 1990, **8**, 131-151.
4. K. Vanommeslaeghe, E. Hatcher, C. Acharya, S. Kundu, S. Zhong, J. Shim, E. Darian, O. Guvench, P. Lopes, I. Vorobyov and A. D. Mackerell Jr., *Journal of Computational Chemistry*, 2010, **31**, 671-690.
5. J. Wang, R. M. Wolf, J. W. Caldwell, P. A. Kollman and D. A. Case, *J Comput Chem*, 2004, **25**, 1157-1174.
6. W. L. Jorgensen and J. Tirado-Rives, *Proceedings of the National Academy of Sciences of the United States of America*, 2005, **102**, 6665-6670.